Carbohydrate Polymers 110 (2014) 302–308

Contents lists available at ScienceDirect

Carbohydrate Polymers

journal homepage: www.elsevier.com/locate/carbpol

In situ synthesis of MnO_2 coated cellulose nanofibers hybrid for effective removal of methylene blue

Yaru Wang, Xiaofang Zhang, Xu He, Wei Zhang*, Xinxing Zhang, Canhui Lu*

State Key Laboratory of Polymer Materials Engineering, Polymer Research Institute at Sichuan University, Chengdu 610065, China

ARTICLE INFO

Article history:
Received 7 January 2014
Received in revised form 21 March 2014
Accepted 2 April 2014
Available online 18 April 2014

Keywords:
Manganese dioxide
Cellulose nanofibers
Nanocomposites
Decolorization of methylene blue

ABSTRACT

A one-step and energy-efficient synthetic method was developed to fabricate manganese dioxide (MnO_2)/cellulose nanofibers (CNFs) hybrid. In this process, bamboo CNFs acted as both a reducing reagent for the Mn (VII) and an ultralight support for the generated MnO_2 nanosheets. Neither additional reducing reagents nor heating were adopted during the synthesis process. The phase constitutions, crystal structure and morphology of the hybrid were systematically investigated. Both oxidative and adsorptive decolorization of methylene blue (MB) were investigated to evaluate its efficiency on dye wastewater treatment. The results showed that the few-layer MnO_2 nanosheets deposited on CNFs exhibited high decolorization efficiency for the oxidation and adsorption of MB. When slurry containing 25 mg MnO_2/CNFs hybrid was dispersed in 25 mL 80 mg L^{-1} MB solution, the removal of MB was more than 99.8% within 2 min.

1. Introduction

Methylene blue (MB), a representative of dyestuffs resistant to biodegradation (Chowdhury, Azam, Aktaruzzaman, & Rahim, 2009), has various dangerous effects on human and animals. It can cause heart rate increasing, nausea and vomiting (Hassan, Abdel-Mohsen, & Fouda, 2014). Dye removal by physical and chemical methods, such as coagulation, ultra-filtration, electro-chemical adsorption and photo-oxidation, has been studied extensively (Parkansky, Simon, Alterkop, Boxman, & Berkh, 2013). However, wastewater treatment is a costly yet important task for process industries due to the straighten regulations in most of the countries (Rehman, Kim, & Han, 2012). Thus, an energy-saving and low cost method for the removal of cationic dyes from industrial effluents is still an important and challenging subject in the field of environmental remediation (Zhou, Fu, Liu, Yang, & Zhan, 2011). Recently, the development of nanoscience and nanotechnology suggests that many of the current water-treatment problems might be resolved or greatly ameliorated by using nanosorbents, nanocatalysts, bioactive nanoparticles, catalytic membranes with nanostructures and so on (Chen & He, 2008). Among them, nanosized manganese oxides (MnO_x) could be one of the promising materials as adsorbents or catalysts for the removal of organic pollutants from water by adsorption and subsequent catalytic combustion at relatively low temperatures (Liu, Liu, Zhao, Qu, & Zhang, 2010).

For the MB degradation reactions, nano-MnO_x usually performs as a catalyst with H_2O_2, though a few literatures reported degradation without H_2O_2 (Hao et al., 2013). In fact, MnO_x has versatile functions for the MB removal: (i) catalyzing the oxidation of MB with H_2O_2 (Zhang et al., 2006), TBHP (Sriskandakumar et al., 2009) or O_2 (Kuan & Chan, 2012), etc.; (ii) physical adsorption; (iii) acting as an oxidizing reagent of itself. However, most of the synthesized MnO_x is in powder or colloid form, especially the nanosized ones. It has encountered several engineering limitations: (i) difficulty in solid–liquid separation; (ii) leaching of nanoparticles along with the treated effluent (Maliyekkal, Lisha, & Pradeep, 2010); (iii) ease of aggregation after using and thereby low reuse value.

Aggregation of nanoparticles and dust pollution can be avoided by anchoring the nanoparticles on suitable matrices. Cellulose fibers are considered as one of the favorite candidates. Natural cellulose fibers are one of the most important natural polymers, an almost inexhaustible raw material, and a key source of sustainable materials on an industrial scale (Klemm et al., 2011). Cellulose nanofibers (CNFs) have been extensively employed as a preferential support material due to its high surface area (Sehaqui, Zhou, & Berglund, 2011), low density (Lavoine, Desloges, Dufresne, & Bras, 2012), and environmental friendliness. Though previous works have reported $KMnO_4$ as an effective initiator for the graft copolymerization of some vinyl monomers onto cellulose (Pashkuleva, Marques, Vaz, & Reis, 2005) and the chemical changes after the

* Corresponding authors. Tel.: +86 28 85460607; fax: +86 28 85402465.
E-mail addresses: weizhang@scu.edu.cn (W. Zhang), canhuilu@263.net (C. Lu).

http://dx.doi.org/10.1016/j.carbpol.2014.04.008
0144-8617/

grafting reaction, the final byproducts of MnO_x have rarely been utilized.

In this study, the nano-MnO_2 deoxidized from $KMnO_4$ by bamboo cellulose fibers was first used in the MB decolorization. We proposed a new approach using nanofibrillated bamboo fiber networks as the support for the non-agglomerated synthesis of MnO_2/CNFs hybrid. Furthermore, CNFs were not only used as a suitable support and a reducing reagent but also a synergetic adsorbent when treating MB in water. The hybrid showed improved decolorization performance with both high oxidative and adsorption efficiency. This material exhibited great potential for environmental rehabilitation.

2. Experimental

2.1. Materials

Never-dried bamboo (*Phyllostachys pubescens*) pulp was kindly provided by Yongfeng Paper Co., Ltd, Muchuan, China. Potassium permanganate, sodium hydroxide, ethanol, manganese dioxide (MnO_2) and methylene blue purchased from Kelong Company (Chengdu, China) were all of analytic grade.

2.2. CNFs preparation

The CNFs were extracted from bamboo pulp fibers according to the literature (Chen, Yu, & Liu, 2011). Briefly, the never-dried pulp was soaked and dispersed in distilled water at a concentration of approximately 0.05 wt%. About 150 mL of the suspension was then sonicated using a horn type ultrasonic generator (JY98-IIID, Ningbo Scientz Biotechnology Co., Ltd., China). The sonication was conducted at an output power of 1200 W for 60 min in an ice/water bath.

2.3. Preparation of MnO_2/CNFs hybrid

20 mL 0.5 mol L^{-1} alkaline permanganate ($KMnO_4$:NaOH = 1:1 in molar ratio) solution was mixed with 300 mL 1 wt% bamboo CNFs suspension and stirred at room temperature for 8 h to get the in situ grown MnO_2/CNFs hybrid. The product was then washed with distilled water to remove any possible residual reactants. Finally, the clean hybrid was redispersed in water by stirring and the solid concentration of the wet slurry was 9.3 wt%. The sample was kept wet all the time to avoid irreversible agglomeration of the hybrid.

2.4. Material characterization

X-ray diffraction (XRD) patterns were used to identify the phase constitutions and crystal structure of the as-prepared hybrid and CNFs. The patterns were recorded from $2\theta = 5–80^\circ$ on an X'Pert X-diffractometer (Philips Co., Netherlands) using Cu-K_α radiation ($\lambda = 0.1540$ nm) operated at 40 kV and 40 mA. The crystallinity index (CrI) of original bamboo CNFs and those in the hybrid was calculated using the Segal method (Segal, Creely, Martin, & Conrad, 1959). In order to determine the crystalline structure of MnO_2, the MnO_2 nanosheets were separated from CNFs. The purified specimen of MnO_2 was prepared through the following procedure: the slurry of MnO_2/CNFs hybrid was solvent exchanged with methyl alcohol and kept soaking in methyl alcohol for 1 h. Then the 'activated' CNFs with MnO_2 on the surface was solvent exchanged with dimethylacetamide (DMAc), followed by mixing with DMAc/LiCl (8 wt% LiCl concentration) under agitating for one day until the cellulose was completely dissolved. The cellulose solution and MnO_2 was separated by centrifugation and washing with DMAc/LiCl repeatedly. XPS (X-ray photoelectron spectroscopy) signals were collected on a VG Micro MK II instrument. The hybrid was dried at 80 °C before examination. The surface morphology of bamboo CNFs and MnO_2/CNFs hybrid was characterized using a transmission electron microscope (TEM) (Tecnai G2 F20 S-TWIN). The FTIR spectra were recorded from 4000 to 400 cm^{-1} at a resolution of 4 cm^{-1} over 20 scans on a Nicolet 6700 FTIR spectrophotometer (USA). The amount of MnO_2 in the MnO_2/CNFs hybrid was evaluated using flame atomic absorption spectroscopy (AAS) (VARIAN Co., USA). The produced hybrid slurry was dried at 80 °C in an oven before decomposition of the organics with concentrated HNO_3 and $HClO_4$ (Gerritse & Van Driel, 1984). After appropriate addition of HCl and water, the resulting solution was analyzed by flame AAS.

2.5. Decolorization of MB

The obtained MnO_2 coated CNFs were used to remove the MB dye. Typically, 286 mg wet hybrid slurry containing 25 mg solid MnO_2/CNFs hybrid was added to 50 mL beakers containing 25 mL 80 mg L^{-1} MB solution and stirred at room temperature. Initial pH of the system was adjusted in the range from 3.1 to 9.6. At each pre-determined time interval, the solution was suctioned off by a syringe with a 0.22-μm syringe-end filter and the MB concentrations of filtrates were then determined using a MAPADA UV-1800 spectrophotometer at $\lambda_{max} = 664$ nm (Zhang et al., 2001). In the case of high MB concentrations which outranged the measurement limit of the facilities, the MB solutions were diluted using deionized water. The decolorization efficiency of MB was measured by the concentrations at different time intervals. Decolorization efficiency, (A_t) (%), was defined as $(A_t)(\%) = (A_0 - A_t)/A_0 \times 100\%$, where A_0 was the initial concentration of MB and A_t was the concentration at contact time of t. For comparison, 25 mg pure CNFs and 25 mg commercial MnO_2 were tested in parallel under the same conditions as the above. To evaluate the effects of gaseous environment and H_2O_2 on MB decolorization, 25 mL MB solution (80 mg L^{-1}) was reacted with 25 mg MnO_2/CNFs hybrid in a flask reactor under N_2 protection. The MB solution was nitrogen bubbled for 30 min before the hybrid was added in order to remove the dissolved O_2 in the solution. Besides, 12.5 mL of 30 wt% H_2O_2 was mixed with 12.5 mL of 160 mg L^{-1} MB solution and examined using above mentioned method. For comparison purpose, 12.5 mL 160 mg L^{-1} MB was mixed with 12.5 mL cellulose suspension (containing 25 mg CNFs) under pH 9.6 and the MB concentration was determined in the same way as for other samples. The concentrations of soluble Mn(II) in the MB solutions at different pHs and time intervals during the decolorization process were determined by atomic absorption spectrometry (AAS) (VARIAN Co., USA).

3. Results and discussion

3.1. Characterization of the MnO_2/CNFs hybrid

3.1.1. Mechanisms of MnO_2/CNFs hybrid formation

Permanganate ion is a strong oxidizing reagent which still remains as one of the most versatile and vigorous multiequivalent oxidants used for the oxidation of inorganic and organic compounds (Hassan, Dahy, Ibrahim, Zaafarany, & Fawzy, 2012). Mechanisms for the reaction between polysaccharides and $KMnO_4$ have been proposed in the previous literatures (Hassan, 1993; Hassan et al., 2012; Khairou, 2003) (see Scheme 1). First, cellulose alkoxide was formed by deprotonation of the cellulose macromolecules with sodium hydroxide [Eq. (1), Scheme 1]. Then oxidation of cellulose by permanganate ion occurred in strongly basic solutions through the formation of an intermediate complex involving Mn (VI) as a transient oxidation state of manganese [Eq. (2)] (Khairou, 2003). Cellulose, as both a deoxidizer and a supporter, was functionalized with permanganate groups in the alkaline

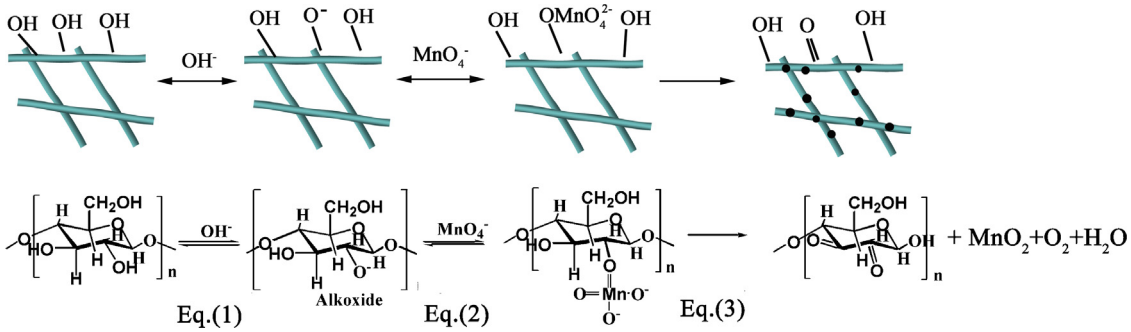

Scheme 1. The preparation of MnO_2/CNFs hybrid and its formation mechanism.

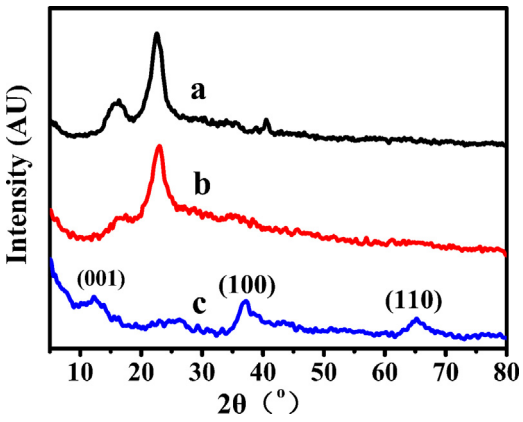

Fig. 1. XRD patterns of pure CNFs (a), MnO_2/CNFs hybrid (b), and MnO_2 separated from the hybrid (c).

condition here. When the concentration of Mn (VI) built up, a slow decay of the intermediate took place to give rise to the final MnO_2 and at the same time cellulose was converted into ketones as final products [Eq. (3)] (El-Khatib, 2002). Heterogeneous reaction only occurred on the surface of cellulose. As a result, a thin coating of generated MnO_2 nanolayer was deposited on the surfaces of CNFs.

3.1.2. Structure and morphology of the MnO_2/CNFs hybrid

Fig. 1 gives the XRD patterns of the pure CNFs, MnO_2/CNFs hybrid and the pure MnO_2 separated from the hybrid. The results confirmed the formation of layered birnessite with a turbostratic structure (Chen & He, 2008). Both CNFs and MnO_2/CNFs hybrid showed peaks around $2\theta = 16^\circ$ and 22.4°, which were believed to represent the typical cellulose I structure (Chen et al., 2011). The CrI of original bamboo CNFs and those in the hybrid were 87 and 77, respectively. The decrease of CrI for bamboo CNFs in the hybrid was probably due to the damage of the cellulose crystalline region with the alkaline $KMnO_4$ treatment. However, a further identification of the MnO_x was difficult due to their low crystallinity with weak and broad diffraction peaks which were overlapped by cellulose peaks. In order to determine the crystalline structure of MnO_x on CNFs, MnO_x were detached from the hybrid by dissolving cellulose in DMAc/LiCl solution (Zhu, Wang, & Zhou, 2008). The predominant peaks corresponding to diffractions of the (0 0 1), (1 0 0) and (1 1 0) lattice planes were all indexed to layered birnessite with a turbostratic structure. Due to the poor crystallization, this as-obtained MnO_2 were expected to have large surface area, strong adsorbing power, and high redox activity (Zhu et al., 2008).

The MnO_2/CNFs hybrid was subjected to XPS analysis and the results from Mn 2p, O 1s and C 1s core levels are shown in Fig. 2. Two major peaks at 653.5 and 641.7 eV in the Mn 2p XPS spectrum suggested that Mn was present in its IV state (Kalubarme, Cho, Yun, Kim, & Park, 2011; Xing, Yu, Xu, Wu, & Li, 2008). The energy separation of 11.8 eV was in quantitative agreement with the reported data for Mn 2p3/2and Mn 2p1/2 in MnO_2 (Xing et al., 2008). The O 1s spectra can be fitted with three components, which were respectively related to lattice oxygen (529.2 eV) (Garcia et al., 2012) for the MnO_x, Mn—OH bond (531.1 eV) for a hydrated trivalent oxide and the H—O—H bond (532.5 eV) for residual water (Dai, Wang, Zhao, & Xie, 2006). The line peak at 284.6 eV was due to the reference carbon of the hydrocarbon (Rodrigues-Filho, Gushikem, Gonçalves, Cachichi, & de Castro, 1996). For cellulose, C peak at 287.8 eV was attributed to C=O (Pasquini, Teixeira, Curvelo, Belgacem, & Dufresne, 2008), and the C peak at 286.3 eV peak was for —C—C—O— (Pashkuleva et al., 2005). Based on the above discussion, MnO_2 was presented in the hybrid.

The FT-IR spectra of CNFs and MnO_2/CNFs hybrid were shown in Fig. 3. Both spectra revealed the characteristic absorption peaks of cellulose. The 4000–2995 cm^{-1} regions were attributed to O—H stretching of cellulose. The peaks at 1050 and 899 cm^{-1} were assigned to the C—O stretching and C_1—H deformation vibrations in cellulose, respectively (Chen et al., 2011). Especially, the enhanced peak at around 1050 cm^{-1} was caused by the vibration of the hydroxyl groups combined with Mn atoms (Kang, Lim, & Shin, 2006). A dominant peak of Mn—O stretching vibrations at

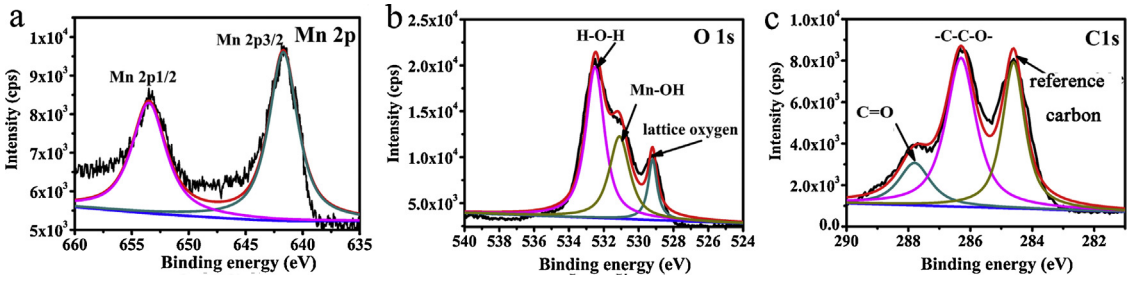

Fig. 2. XPS spectra of the MnO_2/CNFs hybrid: the fitted spectra of Mn 2p levels (a), the fitted spectra of O 1s levels (b) and the fitted spectra of C 1s (c).

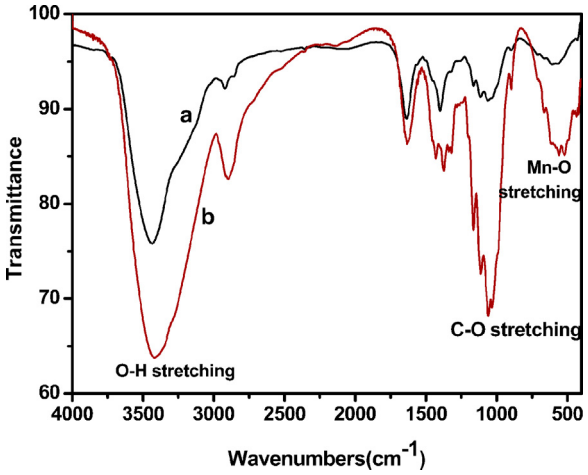

Fig. 3. FT-IR spectra of the bamboo CNFs (a) and MnO_2/CNFs hybrid (b).

approximately 400–750 cm^{-1} (Feng, Kanoh, Miyai, & Ooi, 1995) was observed in the spectra of MnO_2/CNFs hybrid. This proved the presence of MnO_x in the hybrid nanomaterial.

Fig. 4 showed the digital photographs of the original CNFs and MnO_2/CNFs hybrid. The color of CNFs changed from white to brownish black, suggesting the formation of MnO_2 on the surface of CNFs. This result was in good agreement with TEM images. TEM images of bamboo CNFs (Fig. 4a) and MnO_2/CNFs hybrid material (Fig. 4b and c) at different magnifications were acquired. The CNFs have still kept its original fibroid morphology after the chemical reactions. Meanwhile, turbostratic birnessite has grown on the fibers' surface (shown in Fig. 4b and c), resulting in some deeper color segments on the fibers (shown in Fig. 4b). The nanostructured agglomerates in fact was comprised of inter-tangled ultrathin nanosheets with the dimension about 19 nm in edge length and 1.8 nm in thickness as exemplified by Fig. 4c. And the content of MnO_2 in the hybrid was calculated to be 17.3 wt% by AAS analysis.

3.2. Adsorptive decolorization

MB dye solution was discolored rapidly by the as-prepared hybrid material within a wide range of pH value (Figs. 5 and 6). Since the high initial concentration of MB at time 0 min outranged the measurement limit of the instrument, the 80 mg L^{-1} of MB was not shown in the UV-vis spectrum. Instead, a MB solution of 20 mg L^{-1} was set as a reference (black dotted curve in Figs. 5 and 6). Besides, due to the low decolorization efficiency of pure CNFs and commercial MnO_2, MB solutions treated by these materials were diluted 3 and 4 times, respectively. At pH 9.6 and 6.7, fast and almost complete decolorizations of MB by the hybrid were achieved within 5 min. The removal efficiencies were demonstrated by UV-vis absorption spectra (Fig. 5a and b) and photographs (inserted image in Fig. 5b) recorded at the 0 and 5 min, respectively. No shifts of the characteristic peaks with increased contact time were observed, suggesting no intermediate was generated during the interaction of MB dye molecules with MnO_2/CNFs hybrid. The decrease in peak intensity was totally attributed to the MB adsorption by the hybrid material. The as-obtained MnO_2/CNFs hybrid, the CNFs without any modification (Fig. 5c) and commercial MnO_2 (Fig. 5d) could adsorb over 99.9%, 37.5% and 16.0% of MB within 5 min under stirring. Furthermore, the MnO_2/CNFs hybrid exhibited better adsorption efficiency at pH 9.6 than that at pH 6.7 (Fig. 5e). Based on the above results, the adsorption efficiency was on the order of adsorption at pH 9.6 > pH 6.7, and hybrid ≫ CNFs > commercial MnO_2. The extremely high decolorization efficiency could be ascribed to (i) excellent water dispersion ability of CNFs, (ii) special lamellar morphology of MnO_2 and (iii) the large surface area of the layered MnO_2 nanosheets. When pH > pH_{zpc} (Zero point of charge) (Zhu, Wang, Xu, & Li, 2010), the surfaces of MnO_2/CNFs hybrid were negatively charged, which was conducive to the adsorption of MB cations. The decolorization process at pH 9.6 in air was almost 140 times faster than that obtained by using δ-MnO_2-coated montmorillonite as the oxidative degradant (Zhu et al., 2010) and 80 times that from the mechanically grounded pelagite (Zhu, Wang, & Zhou, 2008). A list of representative studies is given in Table 1. The hybrid has much higher decolorization efficiency compared with most of previous works (Zaied, Peulon, Bellakhal, Desmazieres, & Chaussé, 2011; Zhu et al., 2010).

3.3. Oxidative decolorization

For a heterogeneous redox reaction, high adsorbing power and redox activity of the solid phases involved are two critical factors influencing the reaction rate (Zhu et al., 2010). The formation of surface precursor complexes via adsorption on MnO_x is postulated to be the prerequisite to oxidation of organic compounds (Zhu et al., 2010).

Oxidative degradation activities of the MnO_2/CNFs hybrid were evaluated by degrading MB under different pH values and different gaseous environments. And the effect of H_2O_2 was also considered. For the initial pH of 3.1 and 4.7 (Fig. 6a and d), 1 min of reaction time was enough for the characteristic peaks of MB dye absorbance at the wavelength of 664 nm to vanish. However, some other peaks have emerged. This evident blue shift of λ_{max} (Table 2) implied possible formation of new compounds in the degradation processes. The characteristic λ_{max} of the possible intermediates in the degradation process were Azure A (AA, 620–634 nm), Azure B (AB, 648–665 nm), and Azure C (AC, 608–622 nm) (Xu et al.,

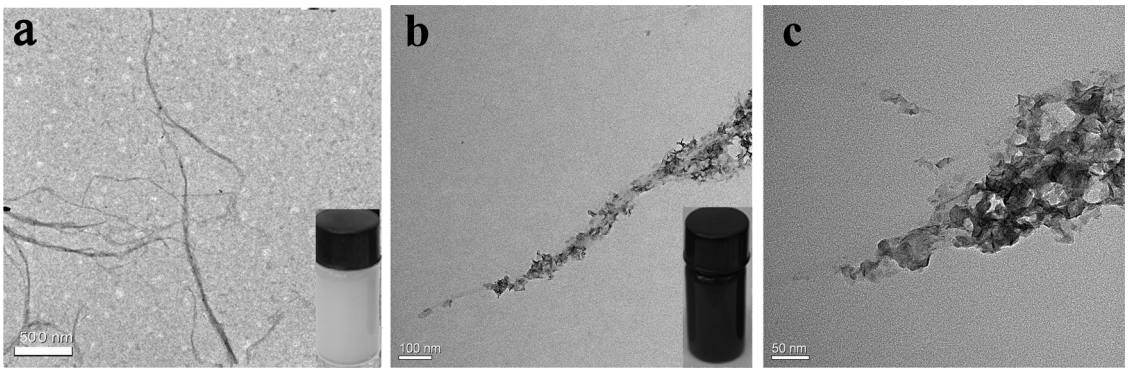

Fig. 4. TEM image of CNFs (a) and MnO_2/CNFs hybrid at different magnifications (b and c). Scale bar = 500 nm (a), 100 nm (b) and 50 nm (c). Insert of TEM image (a) and (b) shows the digital photographs of the original CNFs and MnO_2/CNFs hybrid, respectively.

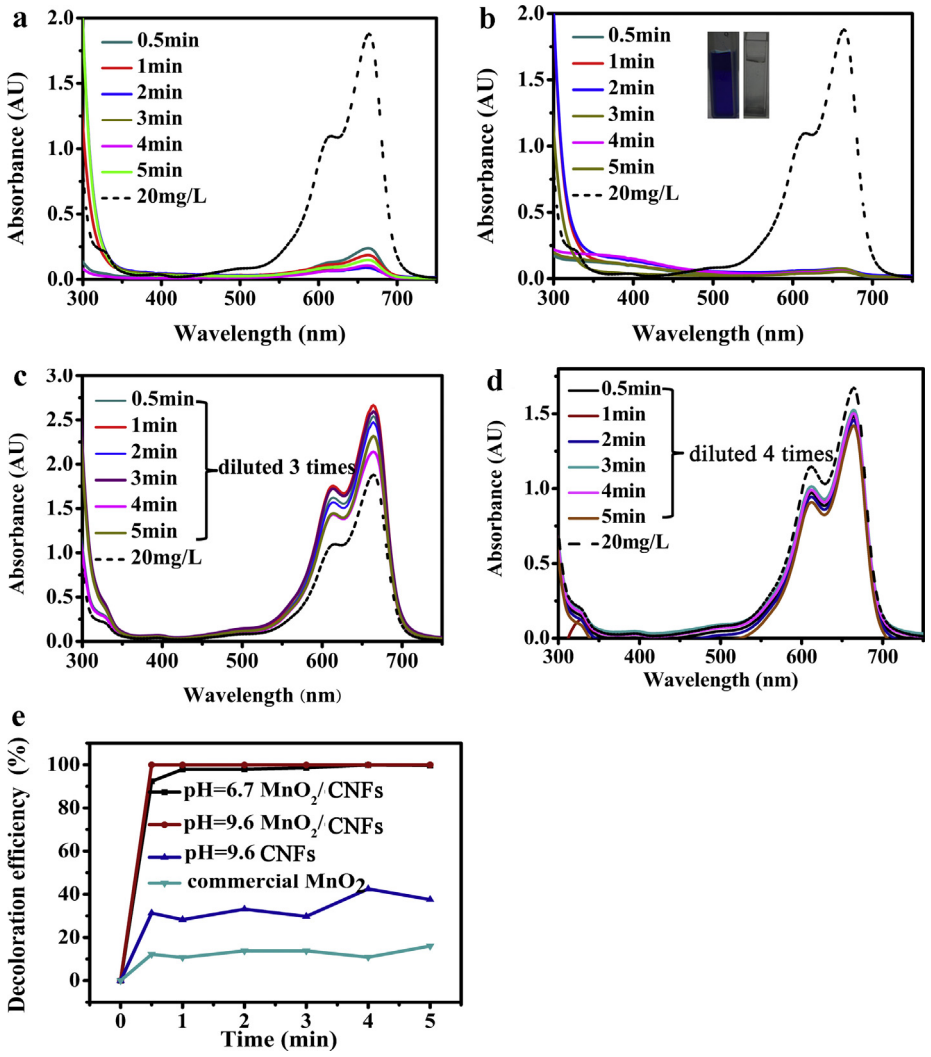

Fig. 5. Changes in the UV–vis absorbance spectra of MB dye after different time intervals at room temperature by the adsorption of hybrid at pH 6.7 (a), hybrid at pH 9.6 (b), CNFs at pH 9.6 (c), and commercial MnO_2 at pH 9.6 (d) and their decolorization efficiency (%) versus time (e). Insert of (b) shows the digital photographs of the initial MB color of 80 mg L^{-1} and the color after 5 min adsorption by hybrid at pH 9.6.

2008). According to Lee's report, the 620 nm was the isosbestic point of the MB monomer/dimer equilibrium (Lee, Sung, & Park, 1999). This decolorization at pH values of 3.1 and 4.7 in this work might not result from pure adsorption but the oxidation by MnO_2 which led to oxidative cleavage of MB through N-demethylation (Kuan & Chan, 2012). Acid has been found to exhibit either promotive or inhibitive effect on the oxidation of organics by MnO_x (Zhu et al., 2010). The decrease of initial pH usually suppressed the MB adsorption on the surface of the hybrid fiber but increased the potential oxidizing ability of the MnO_2. If the suppressing effects on the MB adsorption dominate, the formation of surface precursor complexes would be inhibited. This was the reason why some of the previous reports concluded that the elevated pH tended to promote the oxidative degradation of MB (Kuan & Chan, 2012). However, in our system, an increased pH would decrease and even deprive the oxidizing ability of the MnO_2. It can be deduced that at pH 3.1, the surface of the layered MnO_2 nanosheets was more positively charged through the protonation reaction than that at pH 4.7. This positive charge would act against the formation of surface precursor complexes. However, the increase in oxidizing power of this system could compensate and even overwhelm the decrease of surface precursor complex due to the decreased pH. Consequently, the decolorization at pH 3.1 was more effective than that at pH 4.3 (Fig. 6e).

Moreover, when a control sample was oxidized in nitrogen environment, the absorbance peaks showed a less remarkable

Table 1
Previous representative studies of MnO_x and MnO_x composites in the application of MB decolorization.

Decolorizing agent	Decolorization efficiency	Amount of decolorizing agent (g L^{-1})	Initial MB concentration (mg L^{-1})	References
MnO_2-coated montmorillonite	90% within 700 min	2	80	Zhu et al. (2010)
Layered MnO_2	>90% within 5 min	2.5	100	Chen and He (2008)
Layered MnO_2 nanosheets, H_2O_2	90% in 20 min	0.2	30	Zhang et al. (2011)
MnO_2/PS foams, H_2O_2	39.9% in 8 min	1.25	25	Wang et al. (2010)
Grounded pelagite	<80% in 400 min	0.6	50	Zhu et al. (2008)
MnO_2 assisted by microwave	99% in 10 min	2	10	Kuan et al. (2013)
MnO_2/CNFs hybrid	99.8% within 2 min	1	80	This study

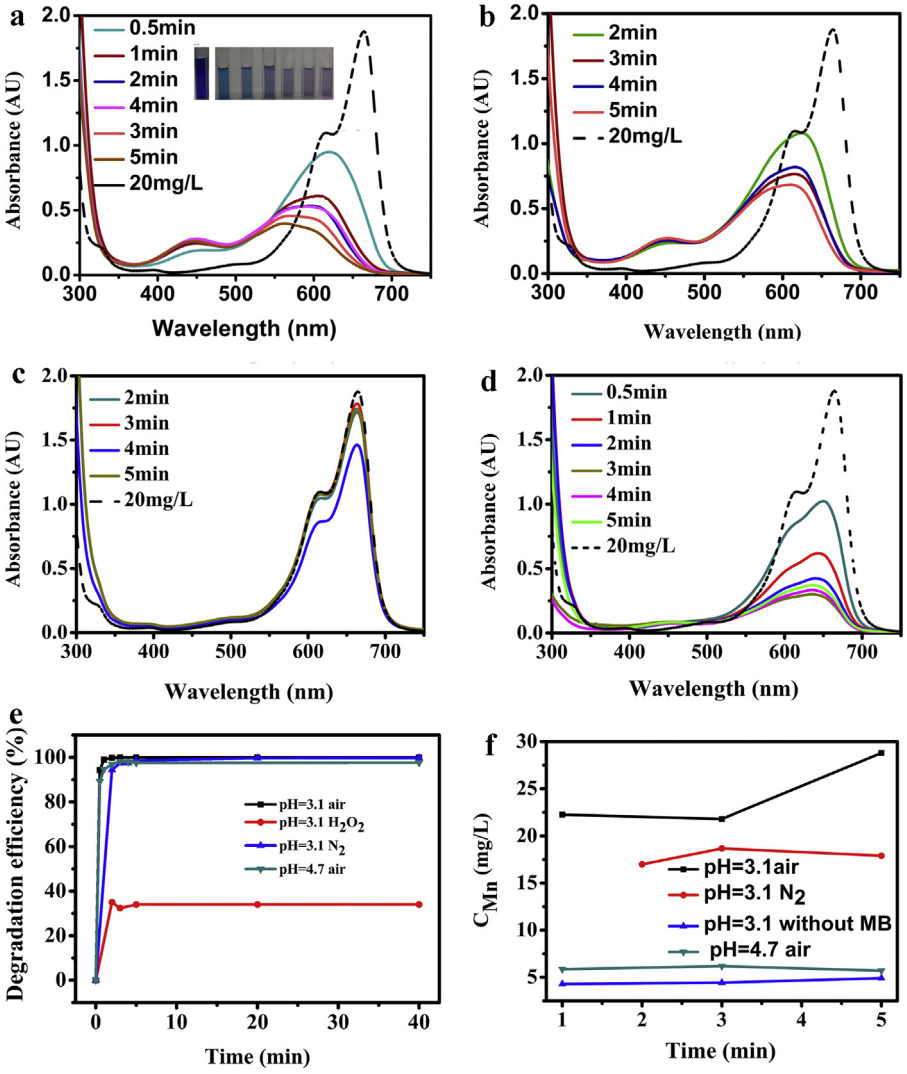

Fig. 6. Changes in the UV–vis absorbance spectra of MB dye after different time intervals at room temperature by the oxidation of hybrid: at pH 3.1 in air (a), pH 3.1 in N_2 environment (b) pH 3.1 with the addition of H_2O_2 in air (c) and pH 4.6 in air (d). And their MB degradation efficiency (%) versus time (e), the concentration of Mn(II) (mg L^{-1}) in the solution versus time (f). Insert of (a) shows the digital photographs of MB color of at time of 0, 0.5, 1, 2, 3, 4, 5 min by contacting with hybrid at initial pH 3.1 in air.

Table 2
The λ_{max} (nm) and Mn (II) (mg L^{-1}) at different time intervals and conditions.

pH and air condition	Time (min)	λ_{max} (nm)	Mn (II) (mg L^{-1})
pH 3.1, air	0.5	620.0	
	1	622.0	22.26
	2	594.0	
	3	562.0	21.80
	4	558.0	
	5	556.0	28.79
pH 3.1, N_2	2	624.0	16.99
	3	616.0	18.68
	4	616.0	
	5	610.0	17.9
pH 4.6, air	0.5	650.0	
	1	644.0	5.86
	2	640.0	
	3	636.0	6.19
	4	636.0	
	5	636.0	5.7

blue-shift but were more intensive compared to that in air atmosphere (Fig. 6b). This was possibly because the oxygen-adsorbed Mn (II) could be surface auto-catalytic oxidized by the dissolved oxygen (DO) in solution to form high valence Mn compounds again. (Kuan, Chen, Hu, & Tzou, 2013). In this condition, MnO_x served as the catalyst and DO acted as the oxidant in reaction (Kuan et al., 2013). The newly formed high valence Mn compounds was also an active adsorbent and oxidant, and may help improve MB adsorption and the following oxidation to some extent (Zhu et al., 2008).

It has been reported that the addition of a catalyst such as MnO_2 to the system with H_2O_2 would lead to higher degradation reaction rates for the effective removal of organics (Zhang, Nie, Hu, & Hu, 2011). However, with H_2O_2 in our system, the absorbance peaks remained at 664 nm and no significant intensity decrease was observed as the reaction time prolonged (Fig. 6c). Therefore, H_2O_2 was not adapted to our degradation system.

Considering the Nernst equation ($MnO_2(s) + 4H^+ + 2e^- \rightarrow Mn^{2+}(aq) + 2H_2O$) (Zhao et al., 2013) and the formation of other dyes during the oxidative decolorization process, the decolorization efficiency could be alternatively expressed by the Mn (II) concentration changes in solutions (Fig. 6f). Since the dissolved Mn (II) concentration at pH 3.1 was maintained at about 4.3 mg L^{-1} in the absence of MB, the increase of Mn (II) concentration in the presence of MB as reaction proceeded was a convictive indicator of oxidative decolorization of MB (Fig. 6f). Besides, the higher Mn(II) concentration at pH 3.1 than that at pH

4.7 was caused by the elevated reductive dissolution at lower pH, which was in good agreement with the results of UV–vis spectra.

4. Conclusion

We demonstrated the successful synthesis of few-layer MnO_2 by a one-step in situ method using bamboo CNFs as both a reducing reagent and a supporting scaffold under alkaline conditions. The as-obtained hybrid material was detected to be thin layered nano-birnessite coated on CNFs. It showed both excellent adsorption and oxidation efficiency in MB decolorization. The pH took a major role in the adsorption and the oxidation process. Acidic pH condition promoted the oxidative decolorization of MB while alkaline pH condition facilitated the physical adsorption. Due to the facile synthesis process and excellent decolorization performance, the MnO_2/CNFs hybrid is promising for industrial applications.

Acknowledgements

The authors would like to thank Natural Science Foundation of China (51303112 and 51203105) and Young Scholar Fund of Sichuan University (2012SCU11074) for financial support of this work.

References

Chen, H., & He, J. (2008). Facile synthesis of monodisperse manganese oxide nanostructures and their application in water treatment. *Journal of Physical Chemistry C*, *112*, 17540–17545.

Chen, W., Yu, H., & Liu, Y. (2011). Preparation of millimeter-long cellulose I nanofibers with diameters of 30–80 nm from bamboo fibers. *Carbohydrate Polymers*, *86*, 453–461.

Chowdhury, A. N., Azam, M. S., Aktaruzzaman, M., & Rahim, A. (2009). Oxidative and antibacterial activity of Mn_3O_4. *Journal of Hazardous Materials*, *172*, 1229–1235.

Dai, Y., Wang, K., Zhao, J., & Xie, J. (2006). Manganese oxide film electrodes prepared by electrostatic spray deposition for electrochemical capacitors from the $KMnO_4$ solution. *Journal of Power Sources*, *161*, 737–742.

El-Khatib, R. M. (2002). Spectrophotometric detection of methyl cellulose–manganate (VI) intermediate complex in the oxidation of methyl cellulose by alkaline permanganate. *Carbohydrate Polymers*, *47*, 377–385.

Feng, Q., Kanoh, H., Miyai, Y., & Ooi, K. (1995). Hydrothermal synthesis of lithium and sodium manganese oxides and their metal ion extraction/insertion reactions. *Chemistry of Materials*, *7*, 1226–1232.

Garcia, T., Sellick, D., Varela, F., Vázquez, I., Dejoz, A., Agouram, S., et al. (2012). Total oxidation of naphthalene using bulk manganese oxide catalysts. *Applied Catalysis A: General*, *450*, 169–177.

Gerritse, R. G., & Van Driel, W. (1984). The relationship between adsorption of trace metals, organic matter and pH in temperate soils. *Journal of Environmental Quality*, *13*, 197–204.

Hao, X., Zhao, J., Zhao, Y., Ma, D., Lu, Y., Guo, J., et al. (2013). Mild aqueous synthesis of urchin-like MnO_x hollow nanostructures and their properties for RhB degradation. *Chemical Engineering Journal*, *229*, 134–143.

Hassan, A. F., Abdel-Mohsen, A. M., & Fouda, M. M. G. (2014). Comparative study of calcium alginate, activated carbon and their composite beads on methylene blue adsorption. *Carbohydrate Polymers*, *102*, 192–198.

Hassan, R., Dahy, A. R., Ibrahim, S., Zaafarany, I., & Fawzy, A. (2012). Oxidation of some macromolecules kinetics and mechanism of oxidation of methyl cellulose polysaccharide by permanganate ion in acid perchlorate solutions. *Industrial & Engineering Chemistry Research*, *51*, 5424–5432.

Hassan, R. M. (1993). Alginate polyelectrolyte ionotropic gels XIV. Kinetics and mechanism of formation of intermediate complex during the oxidation of alginate polysaccharide by alkaline permanganate with a spectrophotometric evidence of manganate (VI) transient species. *Journal of Polymer Science Part A: Polymer Chemistry*, *31*, 51–59.

Kalubarme, R. S., Cho, M. S., Yun, K. S., Kim, T. S., & Park, C. J. (2011). Catalytic characteristics of MnO_2 nanostructures for the O_2 reduction process. *Nanotechnology*, *22*, 395402.

Kang, K. H., Lim, D. M., & Shin, H. (2006). Oxidative-coupling reaction of TNT reduction products by manganese oxide. *Water Research*, *40*, 903–910.

Khairou, K. S. (2003). Kinetics and mechanism of decomposition of intermediate complex during oxidation of pectate polysaccharide by potassium permanganate in alkaline solutions. *International Journal of Chemical Kinetics*, *35*, 67–72.

Klemm, D., Kramer, F., Moritz, S., Lindström, T., Ankerfors, M., Gray, D., et al. (2011). Nanocelluloses: a new family of nature-based materials. *Angewandte Chemie International Edition*, *50*, 5438–5466.

Kuan, W. H., & Chan, Y. C. (2012). pH-dependent mechanisms of methylene blue reacting with tunneled manganese oxide pyrolusite. *Journal of Hazardous Materials*, *239–240*, 152–159.

Kuan, W. H., Chen, C. Y., Hu, C. Y., & Tzou, Y. M. (2013). Kinetic modeling for microwave-enhanced degradation of methylene blue using manganese oxide. *International Journal of Photoenergy*, *2013*, 9, 916849.

Lavoine, N., Desloges, I., Dufresne, A., & Bras, J. (2012). Microfibrillated cellulose – its barrier properties and applications in cellulosic materials: a review. *Carbohydrate Polymers*, *90*, 735–764.

Lee, C., Sung, Y. W., & Park, J. W. (1999). Multiple equilibria of phenothiazine dyes in aqueous cyclodextrin solutions. *Journal of Physical Chemistry B*, *103*, 893–898.

Liu, R., Liu, H., Zhao, X., Qu, J., & Zhang, R. (2010). Treatment of dye wastewater with permanganate oxidation and in situ formed manganese dioxides adsorption: cation blue as model pollutant. *Journal of Hazardous Materials*, *176*, 926–931.

Maliyekkal, S. M., Lisha, K. P., & Pradeep, T. (2010). A novel cellulose–manganese oxide hybrid material by *in situ* soft chemical synthesis and its application for the removal of Pb (II) from water. *Journal of Hazardous Materials*, *18*, 986–995.

Parkansky, N., Simon, E. F., Alterkop, B. A., Boxman, R. L., & Berkh, O. (2013). Decomposition of dissolved methylene blue in water using a submerged arc between titanium electrodes. *Plasma Chemistry and Plasma Processing*, *33*, 907–919.

Pashkuleva, I., Marques, A. P., Vaz, F., & Reis, R. L. (2005). Surface modification of starch based blends using potassium permanganate-nitric acid system and its effect on the adhesion and proliferation of osteoblast-like cells. *Journal of Materials Science: Materials in Medicine*, *16*, 81–92.

Pasquini, D., Teixeira, E. D. M., Curvelo, A. A. D. S., Belgacem, M. N., & Dufresne, A. (2008). Surface esterification of cellulose fibres: processing and characterisation of low-density polyethylene/cellulose fibres composites. *Composites Science and Technology*, *68*, 193–201.

Rehman, M. S. U., Kim, I., & Han, J. I. (2012). Adsorption of methylene blue dye from aqueous solution by sugar extracted spent rice biomass. *Carbohydrate Polymers*, *90*, 1314–1322.

Rodrigues-Filho, U. P., Gushikem, Y., Gonçalves, M. D. C., Cachichi, R. C., & de Castro, S. C. (1996). Composite membranes of cellulose acetate and zirconium dioxide: preparation and study of physicochemical characteristics. *Chemistry of Materials*, *8*, 1375–1379.

Segal, L. G. J. M. A., Creely, J. J., Martin, A. E., & Conrad, C. M. (1959). An empirical method for estimating the degree of crystallinity of native cellulose using the X-ray diffractometer. *Textile Research Journal*, *29*, 786–794.

Sehaqui, H., Zhou, Q., & Berglund, L. A. (2011). High-porosity aerogels of high specific surface area prepared from nanofibrillated cellulose (NFC). *Composites Science and Technology*, *71*, 1593–1599.

Sriskandakumar, T., Opembe, N., Chen, C. H., Morey, A., King'ondu, C., & Suib, S. L. (2009). Green decomposition of organic dyes using octahedral molecular sieve manganese oxide catalysts. *Journal of Physical Chemistry A*, *113*, 1523–1530.

Wang, S., Zhang, Z., Liu, H., Zhang, W., Qian, Z., & Wang, B. (2010). One-step synthesis of manganese dioxide/polystyrene nanocomposite foams via high internal phase emulsion and study of their catalytic activity. *Colloid and Polymer Science*, *288*, 1031–1039.

Xing, X. J., Yu, Y. P., Xu, L. M., Wu, S. X., & Li, S. W. (2008). Magnetic properties of β-MnO_2 thin films grown by plasma-assisted molecular beam epitaxy. *Journal of Physical Chemistry C*, *112*, 15526–15531.

Xu, H., Li, H., Wu, C., Chu, J., Yan, Y., Shu, H., et al. (2008). Preparation, characterization and photocatalytic properties of Cu-loaded $BiVO_4$. *Journal of Hazardous Materials*, *153*, 877–884.

Zaied, M., Peulon, S., Bellakhal, N., Desmazieres, B., & Chaussé, A. (2011). Studies of N-demethylation oxidative and degradation of methylene blue by thin layers of birnessite electrodeposited onto SnO_2. *Applied Catalysis B: Environmental*, *101*, 441–450.

Zhang, T., Oyama, T., Aoshima, A., Hidaka, H., Zhao, J., & Serpone, N. (2001). Photooxidative *N*-demethylation of methylene blue in aqueous TiO_2 dispersions under UV irradiation. *Journal of Photochemistry and Photobiology A: Chemistry*, *140*, 163–172.

Zhang, W., Yang, Z., Wang, X., Zhang, Y., Wen, X., & Yang, S. (2006). Large-scale synthesis of β-MnO_2 nanorods and their rapid and efficient catalytic oxidation of methylene blue dye. *Catalysis Communications*, *7*, 408–412.

Zhang, L., Nie, Y., Hu, C., & Hu, X. (2011). Decolorization of methylene blue in layered manganese oxide suspension with H_2O_2. *Journal of Hazardous Materials*, *190*, 780–785.

Zhao, G., Li, J., Ren, X., Hu, J., Hu, W., & Wang, X. K. (2013). Highly active MnO_2 nanosheets synthesis grapheme oxide templates and their application in efficient oxidative degradation of methylene blue. *RSC Advances*, *3*, 12909–12914.

Zhou, Y., Fu, S., Liu, H., Yang, S., & Zhan, H. (2011). Removal of methylene blue dyes from wastewater using cellulose-based superadsorbent hydrogels. *Polymer Engineering & Science*, *5*(1), 2417–2424.

Zhu, M. X., Wang, Z., Xu, S. H., & Li, T. (2010). Decolorization of methylene blue by delta-MnO_2-coated montmorillonite complexes: emphasizing redox reactivity of Mn-oxide coatings. *Journal of Hazardous Materials*, *181*, 57–64.

Zhu, M. X., Wang, Z., & Zhou, L. Y. (2008). Oxidative decolorization of methylene blue using pelagite. *Journal of Hazardous Materials*, *150*, 37–45.